

RESEARCH PAPER

Dopant-Concentration Dependent Optical and Structural Properties of Cu-Doped ZnS Thin Films

Fatemeh Aghaei¹, Reza Sahraei^{1*}, Ehsan Soheyli², Ali Daneshfar¹

¹ Department of Chemistry, Ilam University, Ilam, Iran

² Department of Physics, Ilam University, Ilam, Iran

ARTICLE INFO

Article History:

Received 12 December 2021

Accepted 18 March 2022

Published 01 April 2022

Keywords:

Cu-doped ZnS thin films

Dopant emission

Nanocrystals

Photoluminescence

ABSTRACT

In this paper, using the chemical bath deposition method and employing the suitable deposition temperature, internal doping of Cu²⁺ ions into nanocrystalline ZnS thin films is reported. X-ray diffraction analysis (XRD) was used to evaluate the structure of the films, which consists of sub-7 nm crystallites of the cubic ZnS. FE-SEM images indicated that the surface morphology of the Cu-doped ZnS films is strongly dependent on dopant level. The influence of the Cu²⁺ ions concentration on optical and specially photoluminescence properties of the Cu:ZnS thin films have been investigated and discussed. Defect-free emission spectra at low deposition temperatures and the appearance of the dopant-related emission peak at higher temperatures demonstrate that this method is an effective strategy for chemical deposition of the Cu-doped ZnS nanocrystals on glass substrates. Furthermore, the concentration quenching effect on photoluminescence intensity has been observed which can be related to non-radiative transitions between electronic energy levels of the neighboring Cu²⁺ ions in the ZnS host lattice.

How to cite this article

Aghaei F., Sahraei R., Soheyli E, Ali Daneshfara . Pluronic based nano-delivery systems; Prospective warrior in war against cancer. J Nanostruct, 2022; 12(2):330-342. DOI: 10.22052/JNS.2022.02.010

INTRODUCTION

The light-matter interaction has been and still is a principal research field for understanding the optical properties of solid-state materials [1]. In this regard, to provide suitable semiconducting thin films with applicable features, it is very important to investigate their optical and surface morphological properties. The optical characteristics of the semiconductor thin films are directly related to their structural and electronic properties, and hence they are very important in optoelectronic devices [2]. Furthermore, light emission is another property that has to be analyzed in pure semiconductor structures. Especially, the origin of the luminescence characteristic in semiconducting

nanocrystals appears from spontaneous radiative recombination of bound electron-hole pairs (excitons) that occurs in the core structure [3]. The spectral range of emission in semiconductor nanocrystals is highly dependent on the type of host matrix and in this respect; zinc sulfide (ZnS) is one of the most technically important structures [4]. The ZnS thin films with a wide direct bandgap and n-type conductivity [5–7] are promising structures for application in optoelectronic devices such as; electroluminescent devices and photovoltaic cells [8–10]. Nonetheless, to stabilize the ZnS system against possible surroundings effects such as optical and chemical corrosions and also to extend the potential areas where the ZnS

* Corresponding Author Email: r.sahraei@ilam.ac.ir



thin films can be applied, the dopant ions have to be introduced. It would help researchers to make certain and desired properties such as wide or narrow bandgap, high optical absorbance, tunable emission color, ferromagnetism, and etcetera [11, 12]. Indeed, the capability of precise control over the doping in semiconductor nanocrystals can create an opportunity for fabricating functional materials with new desirable properties for applications in the real world such as biomedical diagnosis, solar cells, and spintronics [13, 14]. From this point of view, copper ions as a dopant agent can be a good choice for the improvement of the optical, electrical, and structural properties of ZnS thin films [15, 16]. Particularly, impurity states of copper ions can be localized in the mid-gap region and if the doping process was suitable, the emission spectra would show the emission peak related to their energy levels.

Despite the existence of the large variety of deposition techniques such as physical vapor deposition [17], sputtering techniques [18], chemical vapor deposition [19], sol-gel [20], and spray pyrolysis [21], searching the most reliable and economic techniques for deposition of the Cu-doped ZnS thin films has always been the main goal in recent researches. Among these deposition methods, the chemical bath deposition (CBD) is currently attracting a great deal of attention as a relatively simple and cost-effective method. This method does not need sophisticated instruments and vacuum and can also be applied at low temperatures (30–80 °C) to deposit large-scale thin films [22–25]. In addition, it involves chemical reactions in which the precursors are mostly undergoing reactions at the surface or in the vicinity of the substrate.

Up to date, little literature has been reported on the chemical bath deposition of Cu-doped ZnS (Cu:ZnS) thin films [26–29]. Jayanthi et al. reported a CBD-based route for the preparation of ZnS:Cu thin films [26]. Muthukumar et al. studied the structural and photoluminescence properties of ZnS:Cu thin films deposited by the chemical bath method. However, they reported that the hexagonal Cu-doped ZnS films showed an emission peak at about 500 nm, which could arise from the recombination between the shallow donor level (sulfur vacancies) and the t_2 level of Cu^{2+} ions [27]. Ortíz-Ramos et al. have prepared Cu-doped ZnS thin films by CBD method. They reported that the morphology of films is improved with increasing

Cu concentration [28]. Recently, Jrad et al. also studied the effect of Cu concentration on the structural, optical, and electrical properties of ZnS:Cu alloyed thin films. They also determined the electric resistivity, volume carrier concentration, surface carrier concentration, and Hall mobility for obtained alloyed thin films [29]. In recent work, Xu et al. reported chemical bath deposition of p-type transparent conducting thin films of $(\text{CuS})_x:(\text{ZnS})_{1-x}$ nanocomposite. They also fabricated a heterojunction p- $(\text{CuS})_x:(\text{ZnS})_{1-x}/\text{n-Si}$ solar cell with the open-circuit voltage of 535 mV [8]. However, to the best of our knowledge, there are just a few short reports on Cu-doped ZnS thin films prepared by the CBD method. Furthermore, information on the effect of dopant concentration on the emission properties of these films is still limited and needs to be investigated in more detail.

In the present work, the Cu-doped ZnS thin films were chemically deposited in a weak acidic bath (pH of 6.0), in which ethylenediamine tetra-acetic acid disodium salt and thioacetamide act as a complexing agent and a source of sulfide ions, respectively. The main aim of this report is the study of the doping level effect on composition, surface morphology, nanocrystalline structure, optical and photoluminescence properties of the Cu:ZnS thin films, which have been extensively investigated using EDX, FESEM, XRD, UV–Vis, and photoluminescence spectroscopy. In addition, the facility of the suggested method to achieve the internal doping concept is the novelty of the present work which can be useful for the deposition of other metal-doped ZnS thin films.

MATERIALS AND METHODS

Zinc acetate dihydrate $[\text{Zn}(\text{CH}_3\text{COO})_2 \cdot 2\text{H}_2\text{O}]$, copper nitrate trihydrate $[\text{Cu}(\text{NO}_3)_2 \cdot 3\text{H}_2\text{O}]$, ethylenediamine tetra-acetic acid disodium salt (Na_2EDTA), thioacetamide (CH_3CSNH_2), NaOH, Isopropyl alcohol, and HCl which were purchased from Merck Company were of analytical grade and used without further purification. Deionized water was used in all of the cleaning and solutions preparation steps.

Nanocrystalline Cu-doped ZnS thin films were deposited on commercial microscope glass slides and polycrystalline silicon substrates. The substrates were initially cleaned in sulphochromic acid solution and were subsequently washed with deionized water, isopropyl alcohol, and double-distilled water. Then, substrates were transferred

to an oven and dried at 70 °C. The required bath solution was prepared as follows; firstly, desired amounts of 0.05 molL⁻¹ (M) Cu(NO₃)₂ solution were added to the mixture of 6 mL of 1 M Zn(OAc)₂ and 15 mL of 0.2 M Na₂EDTA solutions. The solution pH was about 4.5-5 at different dopant percentages which were increased by the addition of 1 M NaOH to 6. Then 30 mL of 0.4 M thioacetamide solution was slowly added to the above solution. The whole solution was brought to the volume of 100 mL by the addition of deionized water followed by drop-wise addition of NaOH solution for adjusting the pH at 6 again. The dried/clean substrates have been vertically placed in a solution-containing glass tank and immediately transferred to a thermostat bath which has been previously set at three different temperatures of 40, 60, and 80 °C. The deposition solution was kept at the desired temperature for 8 h without any kind of

stirring. The deposited films were finally washed with distilled water and dried in the air at room temperature. The as-prepared films were smooth, uniform, and had good adherence to substrates. The Cu²⁺:Zn²⁺ molar ratio in the deposition solution was varied from 0.0008:100 to 0.75:100.

X-ray diffraction (XRD) measurements were performed to check the crystallinity of the prepared thin films using an automated Philips X'Pert X-ray diffractometer with Cu K α radiation (40 kV and 30 mA). The surface morphology of the Cu:ZnS films was observed by field emission scanning electron microscopy (FE-SEM; Hitachi S-4200) under an acceleration voltage of 15 kV. The thin film's thickness was measured by a Dektak³ profilometer. Energy dispersive x-ray spectroscopy (EDX) was performed using an Oxford INCA II energy solid-state detector equipped with a field emission gun. Room temperature absorption

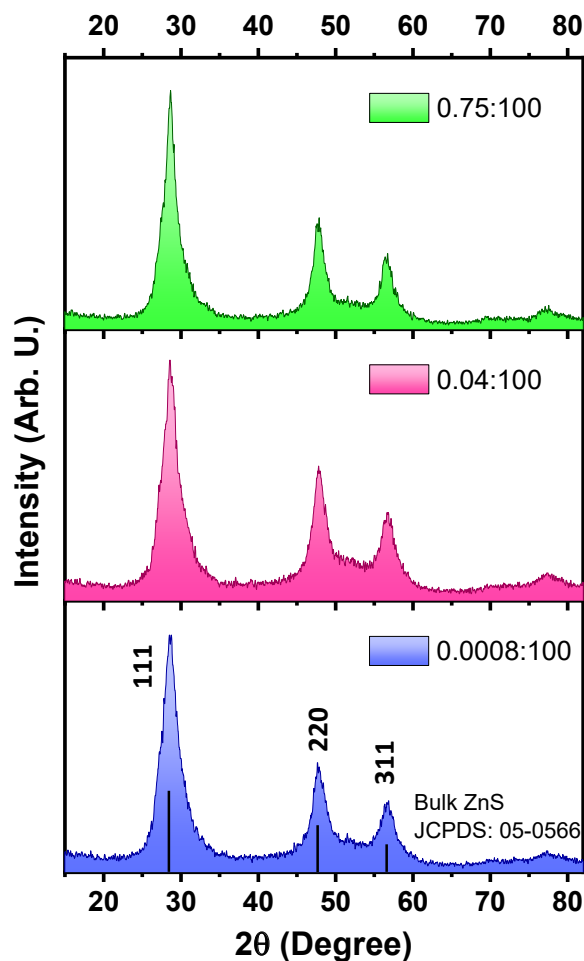


Fig. 1. The XRD patterns of the Cu:ZnS thin films deposited at different Cu:Zn molar ratios and at 80°C for 8 h.

and emission spectra were also recorded using Cary 300 Bio UV-vis and Cary Eclipse fluorescence spectrophotometers, respectively. The thickness of films was also measured by a Dektak profilometer. All measurements were carried out at room temperature.

RESULTS AND DISCUSSION

The XRD patterns of the nanocrystalline Cu:ZnS thin films deposited at different Cu:Zn molar ratios are shown in Fig. 1. The standard XRD pattern for zincblende structure of the bulk ZnS (Joint Committee for Powder Diffraction Standards, JCPDS card no. 05-0566) is given at the bottom of Fig. 1. The XRD peaks are broadened because of the nano-scale size of the structures. As can be seen in Fig. 1, three broad peaks appeared in the diffractogram at around 28.5°, 47.7° and 56.6° reveal the formation of pure-phase polycrystalline Cu:ZnS films with cubic zincblende structure (β-ZnS phase) and good crystalline quality without any noticeable difference to pure ZnS [30]. All the peaks are in good agreement with the Joint committee on powder diffraction standard (JCPDS) data (card no. 05-0566) belonging to the zinc blend ZnS structure. From the XRD profile, no diffracted peaks due to CuS in all patterns have been observed which can be a reason for the presence of the Cu²⁺ impurities as dopant ions.

Although the Scherrer equation is usually employed to estimate particle size, it does not involve the micro-strain present in polycrystalline thin films. The broadening (β_D) in the Scherrer equation represents the broadening related to the

size of particles alone;

$$B_D = \frac{k\lambda}{D\cos\theta} \tag{1}$$

where k is a constant determined by the geometry of the crystallites and it is approximately 0.9 for spherical particles, λ is the wavelength of the used X-ray radiation, D is the average nanocrystallite size, and θ is an angle corresponding to the diffraction maximum. However, the entire contribution to the observed broadening in XRD peaks is owing to the sum of the particle size-related broadening (β_D), broadening due to lattice strain (β_S), and instrumental-related broadening (β_i). The instrumental-related broadening arises from various factors such as non-parallelism of the incident x-ray beam, the presence of other wavelengths apart from Cu-Kα, etc., and it is a constant for a particular experimental setup. Besides, the lattice strain in polycrystalline materials arises from various defects in crystals structure. Thus the experimentally observed broadening (β_e) in x-ray diffraction patterns can be written as [31];

$$\beta_e = \beta_D + \beta_S + \beta_i \tag{2}$$

The broadening due to lattice strain can be written as;

$$\beta_S = 4\epsilon \tan\theta \tag{3}$$

By inserting equations 2 and 3 in equation 1, we could easily derive the Williamson-Hall equation

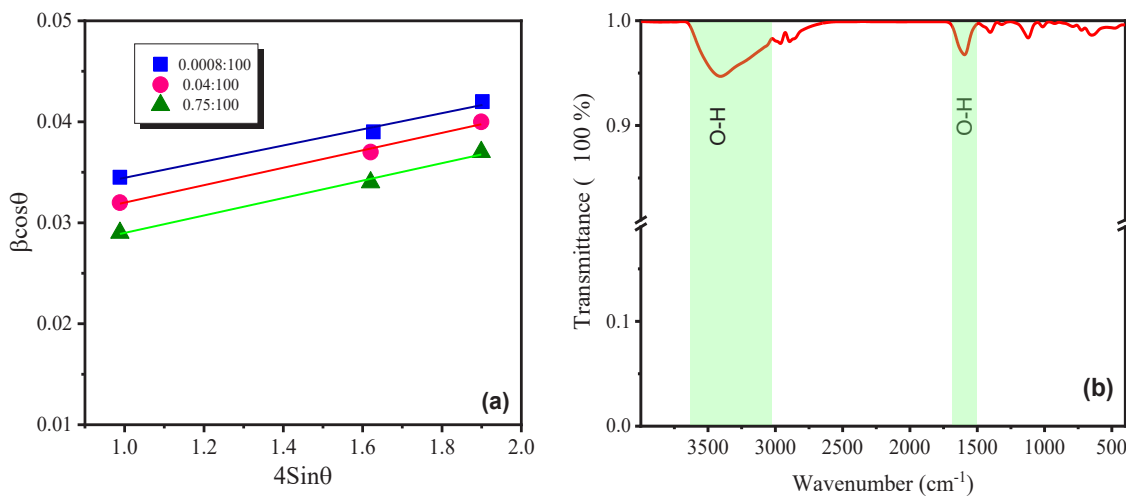


Fig. 2. (a) Plots of βcosθ against 4Sinθ for the Cu:ZnS films deposited at different Cu:Zn molar ratios and at the deposition temperature of 80 °C for 8 h. (b) FT-IR spectrum of the Cu:ZnS films deposited at Cu:Zn molar ratio of 0.04:100.



Table 1. The film thickness, the real Cu:Zn atomic ratios, the average nanocrystallites size, and the lattice strain values for the Cu:ZnS thin films deposited at different Cu:Zn molar ratios and at 80 °C for 8 h.

Cu:Zn molar ratios	Film thickness (nm)	Real Cu:Zn:S atomic ratios	Average nanocrystallite size (nm)	Lattice strain (ε)
0.0008:100	382	0.21:99.6:100	5.3	8.0×10 ⁻³
0.04:100	369	0.66:97.5:100	6.0	8.5×10 ⁻³
0.75:100	378	1.41:95.1:100	6.9	8.6×10 ⁻³

as follow;

$$\beta \cos\theta = \frac{K\lambda}{D} + 4\epsilon \sin\theta \tag{4}$$

where β is the subtraction of the instrumental-related broadening (β_i) from the experimentally observed broadening (β_e), i.e., (β_e - β_i), and it must be corrected using the geometric mean (β = (β_e - β_i) (β_e² - β_i²)^{1/2}), ε is the lattice strain in the films, while all other symbols have the same meaning as in the previous equations. Thus, it is clear that when a linear least-square fit of βcosθ is plotted versus 4sinθ, a straight line with slope ε and intercept kλ/D is obtained, as shown in Fig. 2(a). The values of the lattice strain and the average nanocrystals size for the thin films deposited at different Cu:Zn molar ratios can be calculated from the slope and intercept of these straight lines, respectively. All these values are given in Table 1.

Briefly, it could be concluded from Table 1 that the values of lattice strain (ε) in the case of all Cu:ZnS thin films deposited at different Cu:Zn molar ratios are notably small and it does not change remarkably with alteration in Cu:Zn molar ratios.

These small lattice strain values indicate that the nanocrystals size factor plays an important role in broadening the X-ray diffraction peaks of the Cu:ZnS thin films deposited at different Cu:Zn molar ratios. Moreover, it can be seen that as the Cu:Zn molar ratio increases from 0.0008:100 to 0.75:100, the nanocrystallites size was slightly increased from 5.30 nm to 6.9 nm.

FT-IR spectrum of the Cu:ZnS films deposited at Cu:Zn molar ratio of 0.04:100 has been shown in Fig. 2(b). As it indicates, there is no signal related to the impurities or any other organic species except two very weak peaks related to the stretching and bending vibration modes of O-H groups due

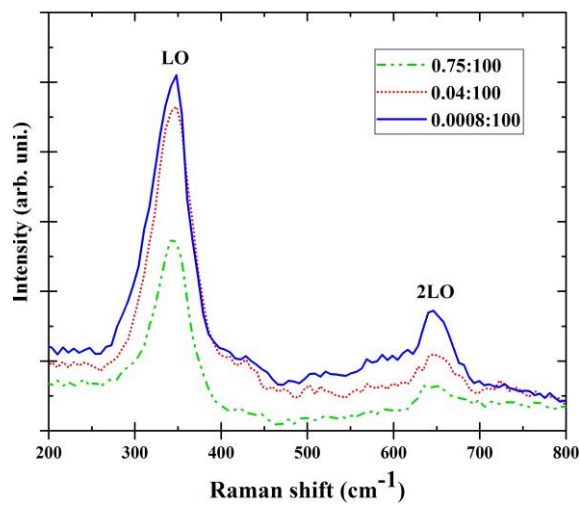


Fig. 3. The Raman spectra of the Cu:ZnS thin films deposited at different Cu:Zn molar ratios and at 80°C for 8 h.

to trace amounts of adsorbed water on the films during the storage time [22].

Fig. 3 shows the Raman spectra of the Cu:ZnS thin films deposited at different Cu:Zn molar ratios and at 80 °C for 8 h. In all spectra, two broadened peaks related to the first- and second-order longitudinal optical phonon vibrations (1LO and 2LO) were observed at around 348 and 652 cm⁻¹, respectively [32]. It is observed that with increasing the Cu:Zn molar ratios in the deposition solution, no shift in the position of Raman peaks occurs, indicating that the predominant β-ZnS phase is preserved. Also, with increasing the Cu content in the films, the intensity of peaks decreases slightly. Similar results have been reported by others [33]. The broadening of peaks could be probably due to phonon confinement as a result

of the nanocrystalline structure of the Cu:ZnS films [33]. It should be noted that no peak related to the phonon modes of CuS has appeared in the spectra. The CuS has two characteristic bands at 270 and 474 cm⁻¹ corresponding to the A_{1g} TO and the S–S bonding stretching [34].

Fig. 4 shows the surface morphology of the Cu:ZnS thin films deposited at different Cu:Zn molar ratios and at 80 °C for 8 h. As can be seen in images, the surface of all thin films is composed of relatively dense and uniform granular grains formed by tightly bound nanocrystals, without the presence of voids, pinholes, or cracks. In addition, with increasing the Cu:Zn molar ratio from 0.0008:100 to 0.75:100, the grain sizes are gradually increased. The same morphology properties for the Cu-doped ZnS thin films

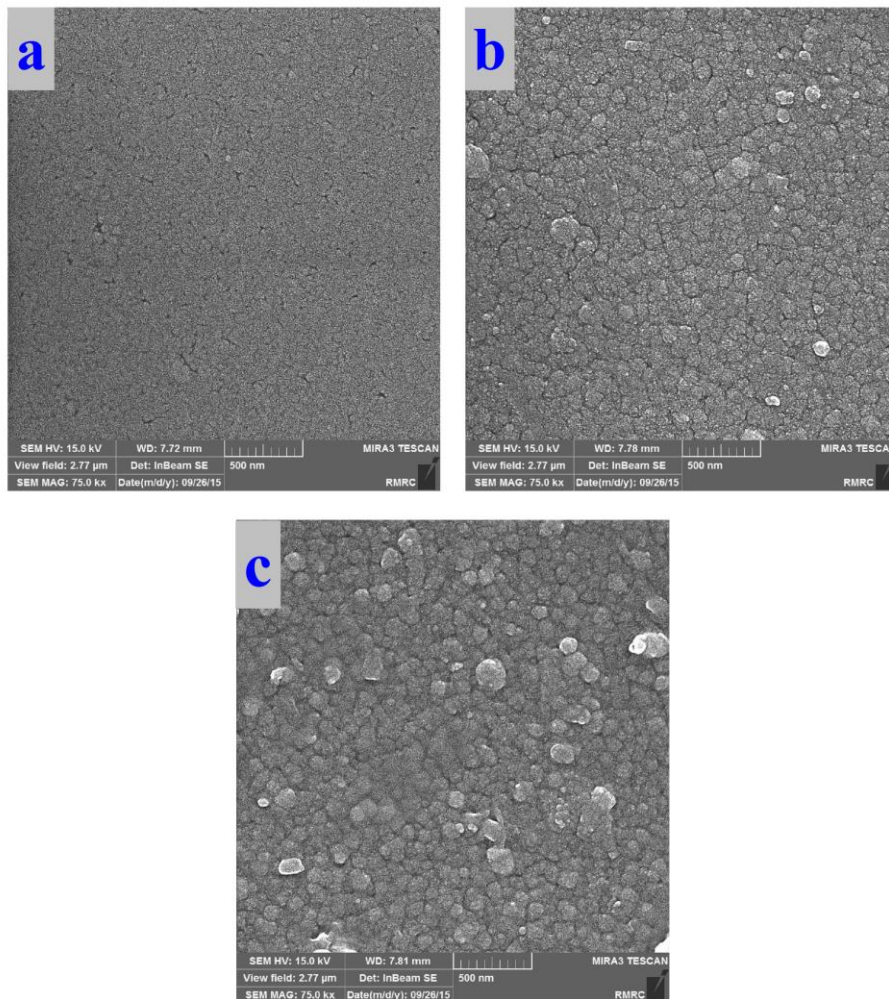


Fig. 4. SEM images of the Cu:ZnS thin films deposited at different Cu:Zn molar ratios: (a) 0.0008:100, (b) 0.04:100, and (c) 0.75:100.

deposited by the CBD method were reported by other researchers [28, 30]. In the CBD method, the formation of the film on a substrate takes place by nucleation and growth processes, where the ionic product of the metallic and sulfur ions exceeds the solubility product [35]. Because the solubility product of CuS (8×10^{-37}) is much less than that of ZnS (1.1×10^{-24}) [36], the addition of Cu^{2+} ions to the deposition solution (increasing of Cu:Zn molar ratio) would lead to a small increase in the nucleation rate and subsequently the faster growth of nanocrystals, resulting in the formation of bigger grains (Fig. 4). The average size of grains (about 100 nm) on the surface of the films is greater than the nanocrystallites size calculated from the XRD results (about 5-7 nm). This is likely because the grains themselves must be a coalescence of the tightly bound nanocrystallites. This phenomenon was also reported by other researchers for the ZnS thin films chemically

deposited on glass substrates [15].

Chemical compositions of the Cu:ZnS thin films were analyzed by the EDX technique. Fig. 5 shows the EDX spectra of the Cu-doped ZnS thin films deposited on a silicon substrate at different Cu:Zn molar ratios and at 80 °C for 8 h. The presence of Zn, S, and Cu-related peaks demonstrate the formation of the Cu:ZnS thin films. The signal of silicon comes from the silicon substrate. It also revealed that the deposited films are close to their stoichiometry. The real Cu:Zn:S atomic ratios of different films were listed in Table 1. For all the films, the atomic percentage of the zinc is less than that of the sulfur. As can be seen, with increasing the nominal Cu:Zn molar ratio used in the deposition solution, the real Zn:S atomic ratio is decreased. In other words, as the amount of Cu dopant increased in the deposited films, the content of the zinc vacancy states in the host lattice (ZnS) is also increased. This observation,

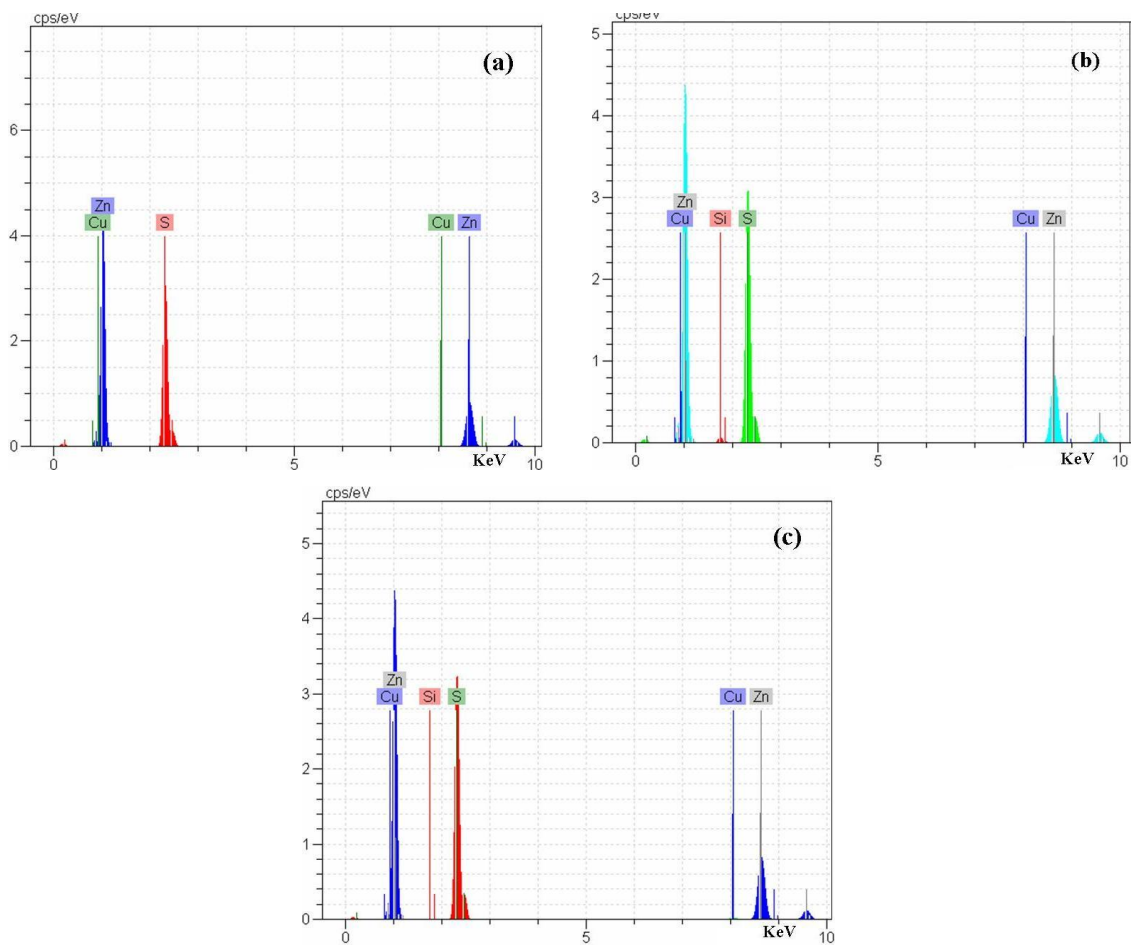


Fig. 5. EDX spectra of the Cu:ZnS thin films deposited on silicon substrate at different Cu:Zn molar ratios: (a) 0.0008:100, (b) 0.04:100, and (c) 0.75:100.

suggests that there can be zinc vacancy states in the lattice structure of the films that are highly effective on emission properties of the Cu-doped ZnS thin films.

When a light beam is incident upon a semiconducting thin film, a fraction of the beam will be reflected, another part will be transmitted through the film, and the rest of the beam will be absorbed. The co-plotting of the transmittance and reflectance spectra for the Cu:ZnS thin films deposited at different Cu:Zn molar ratios has been shown in Fig. 6. As it is clear, the thin films are vigorously transparent at wavelengths larger than 350 nm. Additionally, the sharp increase in the transmittance spectra from 310 nm to 340 nm, exhibits the uniformity and compactness of the crystal structure in the Cu:ZnS thin films [37].

The absorption of photons gives rise to the transition of the electrons from valance band to conduction band. The absorption ability is calculated by its absorption coefficient (α) which is a function of frequency and is defined as;

$$I = I_0 e^{-\alpha d} \tag{5}$$

where I and I_0 are the intensities of the transmitted and incident beams, respectively, and d is the thickness of the film. By calculating the absorption coefficient from the UV-Vis spectra, and employing the Fermi golden law [38], the optical bandgap energy can be estimated by using

the following relation;

$$\alpha h\nu = A(h\nu - E_g)^n \tag{6}$$

where $h\nu$ is the photon energy, E_g is the bandgap energy, A is a constant and it is a function of refractive index and hole/electron effective masses [39]. “ n ” is a constant and related to the type of the transition and in the form of direct allowed transitions, n value is equal to $1/2$ [40]. To determine the direct bandgap energy of the as-prepared films, according to the relation between the absorption coefficient (α) and the incident photon energy ($h\nu$), a plot of $(\alpha h\nu)^2$ as a function of incident photon energy ($h\nu$) is drawn for the Cu:ZnS thin films deposited at different Cu:Zn molar ratios (Fig. 7). Extrapolation of the best fitted straight line to intercept the $h\nu$ axis at $(\alpha h\nu)^2=0$ gives an estimation for optical band gap energies. It is observed that the value of the bandgap energy for the Cu:ZnS thin films decreases from 3.84 to 3.64 eV with increasing the Cu:Zn molar ratio from 0.0008:100 to 0.75:100, respectively. This trend can be attributed to increasing of nanocrystals size as has been shown by XRD analysis. Due to the size dependency of semiconductors’ bandgap energy, the growth of nanocrystals is associated with decreasing the bandgap energy.

Photoluminescence (PL) spectroscopy is a convenient characteristic technique for indicating the energy structure and defects of semiconducting

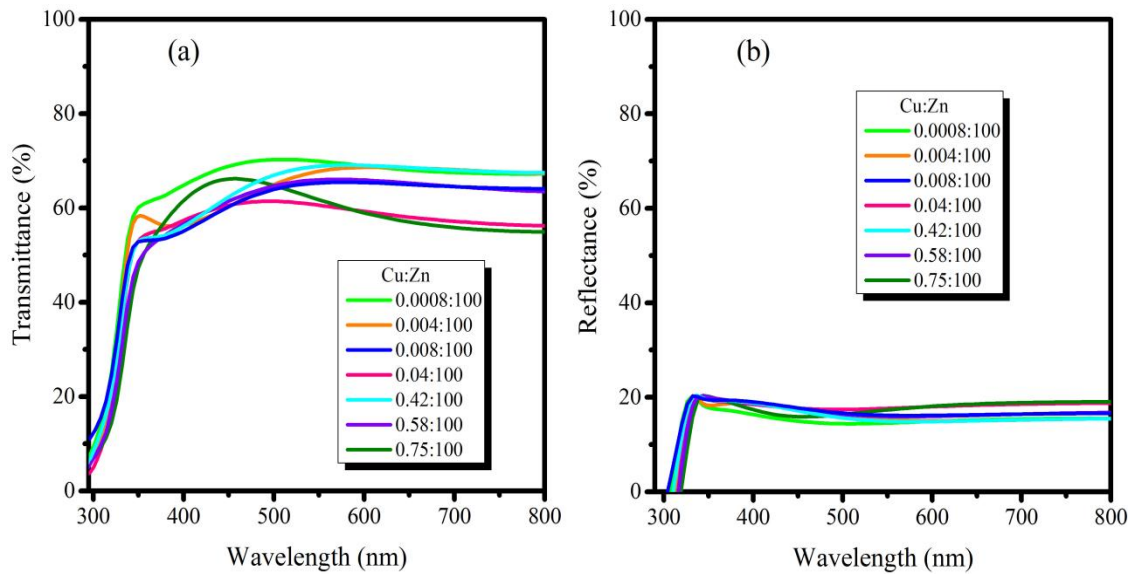


Fig. 6. (a) Transmittance and (b) reflectance spectra of the Cu-doped ZnS thin films deposited at different Cu:Zn molar ratios.

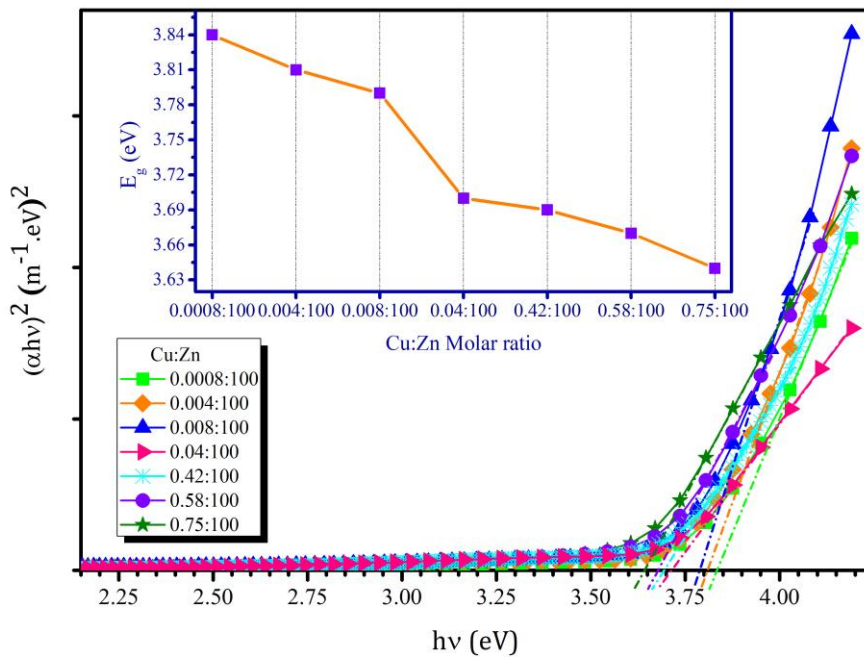


Fig. 7. Plots of $(\alpha hv)^2$ versus $h\nu$ for the Cu:ZnS thin films deposited at different Cu:Zn molar ratios (inset: variation of bandgap energy versus Cu:Zn molar ratio).

thin films. To investigate the effect of deposition temperature on PL emission spectra of the Cu-doped ZnS thin films, different films were prepared at three different temperatures of 40, 60, and 80 °C. As is shown in Fig. 8a, increasing the deposition temperature has three main effects. First, there is a slight red shift by increasing the deposition temperature. This shift would be an ensuing result of easier growth of the nanocrystals, formation of larger nanocrystals and because of the size dependency of the bandgap in semiconductor nanocrystals, it yields to decrease of the bandgap energy and red-shift in PL spectra. The intense peak at about 375 nm can be attributed to excitonic-involved recombination for charge carriers [41]. As is seen in the absorption spectrum (Fig. 8b), the absorption edge has been located at around 345 nm. This is due to the excitation of the electrons from the valence band to the conduction band. By comparing the emission and absorption spectra of the Cu:ZnS thin films prepared at 80 °C and at optimized dopant concentration (Fig. 8b) the small Stokes shift of about 30 nm is observed. This will further suggest that the first emission peak can be assigned to the recombination of the excited electrons in excitonic states with remaining holes in the valence band. Secondly, with increasing the deposition temperature, the overall enhancement

of the emission intensity is observed which indicates the better crystallinity of the thin films prepared at high deposition temperatures. Finally, there is an obvious temperature-dependent variation in PL emission peaks. As is observed, the PL emission spectrum at the low temperature of 40 °C shows a broad excitonic peak located around 370 nm and a small shoulder at about 415 nm which has been attributed to sulfur vacancies [42]. Besides, at low deposition temperatures, Cu^{2+} ions are probably located as surface doping which increases the possibility of non-radiative recombination through the surface trap states and less-intense emission peaks come to pass. However, the initial increase in deposition temperature to 60 °C is accompanied by the appearance of a new emission peak at about 517 nm. Indeed, increasing the deposition temperature leads to the enhancement of the nanocrystals' growth rate. This would increase the formation possibility of zinc vacancy sites as previously showed by EDX results and it can be characterized by the formation of a new pathway for recombination of the charge carriers in the wavelength range of about 517 nm [43]. The most attractive result was observed when the higher deposition temperature of 80 °C was used. At this condition, not only the overall intensity of the emission spectrum increases but also there

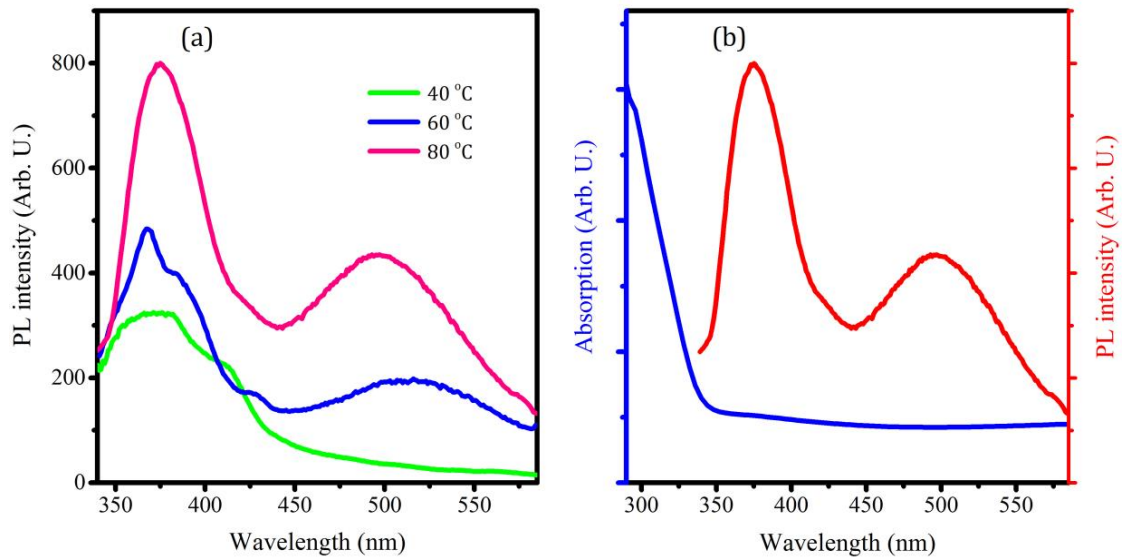


Fig. 8. (a) PL emission spectra of the Cu:ZnS thin films deposited at different deposition temperatures, and (b) absorption/emission spectra of the thin films deposited at 80 °C for 8 h. The Cu:Zn molar ratio in the reaction solution was fixed at 0.04:100.

would be a new emission center at about 500 nm. The possible reason for this observation can be illustrated as follows; Generally, by increasing the deposition temperature, the Cu^{2+} dopant ions adsorbed on the surface of the host ZnS nanocrystals, can diffuse more easily to inside of the host matrix, locate at the Zn^{2+} ion sites and

make their own luminescence centers which are appeared in the mid-gap region. This leads to appearance of the Cu-related peak at 500 nm by substitution of the zinc vacancy sites which is in harmony with the internal-doping concept (Fig. 8a) [42, 44, 45]. Regarding these illustrations, the suggested recombination processes have been

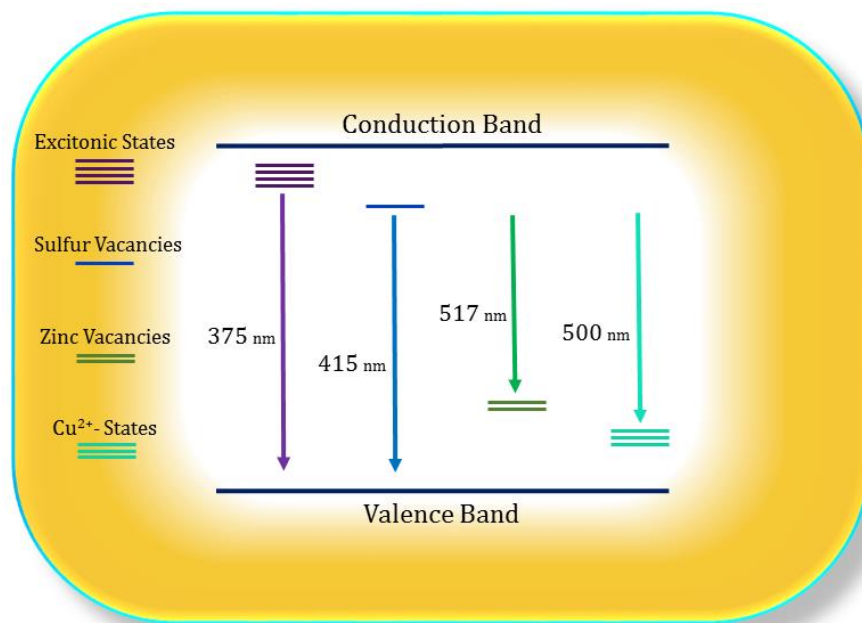


Fig. 9. A proposed depiction for recombination pathways in the present Cu:ZnS thin films.

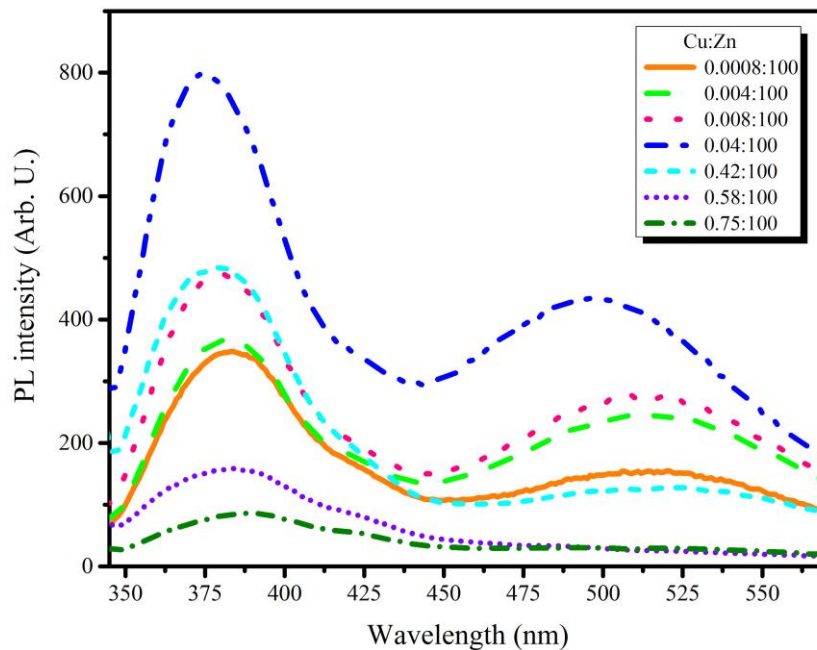


Fig. 10. Effect of Cu:Zn molar ratio on PL emission spectra of the Cu:ZnS thin films deposited at 80 °C for 8 h.

shown in Fig. 9.

The effectiveness of the present method for the preparation of the Cu-doped ZnS thin films is more clear when one takes a look again at the PL emission spectrum at the low deposition temperature of 40 °C. As can be seen, there is approximately no emission peak related to defect states (except a shoulder at 415 nm). Denzler et al. and Haddad et al. [46, 47] recognized four types of defects sites that are present in ZnS structure, which generates four trap levels inside the forbidden energy gap (in the range of 415–520 nm). Based on these results, it can be concluded that the crystallinity of the deposited thin films is high enough, even at low deposition temperatures. But the suitable condition for internal doping of Cu²⁺ ions is provided at higher deposition temperatures.

To obtain the best dopant concentration for emission properties, different amounts of Cu²⁺ ions were used. By incorporation of a higher amount of copper ions, the emission intensity reaches its maximum at Cu:Zn molar ratio of 0.04:100 and then, the PL emission intensity quenches (Fig. 10). This trend would be rational due to non-radiative energy transfer between exceeding dopant levels within the mid-gap region. In this situation, carriers prefer to lose their exciting

energy in a mentioned manner instead of radiative recombination. Such behavior was observed in previous work on transition metal-doped ZnS semiconducting thin films [36]. Besides, when the concentration of dopant increases, the excess amount of dopant ions would locate at the surface of the ZnS nanocrystals through the self-purification phenomenon in such structures [48]. These surface-located impurities may serve as surface defect states and result in non-radiative emission. Hence, the PL intensity, which originates from the radiative recombination possibility in the semiconductor structures, is decreased.

CONCLUSION

A simple CBD method was successfully used for efficient doping of the ZnS thin films by small amounts of Cu²⁺ ions in an ammonia-free bath. Using XRD patterns and the Williamson-Hall equation, the small effect of the strain on the lattice structure of the films was demonstrated. A study of the surface morphology of the deposited films at different Cu:Zn molar ratios by using FE-SEM, showed noticeable adhesiveness with relatively uniform grains distribution. Both of the XRD and FE-SEM analyses, also showed that increasing the Cu:Zn molar ratio leads to a gradual increase in

the grain sizes. The prepared films have optical transmission above 60% in the visible range of the spectrum. Except for the excitonic emission peak in photoluminescence spectra (375 nm), there are three kinds of emission peaks around 410, 517, and 500 nm at different deposition temperatures of 40, 60, and 80 °C, respectively. Based on the PL results in various deposition temperatures, it was concluded that the Cu²⁺ ions are successfully incorporated into the ZnS host matrix at 80 °C. It was found that the PL intensity of the films is strongly dependent on dopant concentration and it increased significantly with increasing the Cu:Zn molar ratio in the precursor solutions, and showed a maximum when the Cu:Zn molar ratio was 0.04:100. The combination of intense violet-green emission, and a simple, low-cost method for deposition of the Cu_xZnS thin films can offer the opportunity for their potential applications in optoelectronic devices such as light-emitting diodes.

CONFLICT OF INTEREST

The authors declare that there is no conflict of interests regarding the publication of this manuscript.

REFERENCES

1. Andreani LC. Light–Matter Interaction: Physics and Engineering at the Nanoscale Light–Matter Interaction: Physics and Engineering at the Nanoscale, John Weiner and Frederico Nunes, Oxford U. Press, 2013. \$110.00 (261 pp.). ISBN 978-0-19-856765-3. Phys Today. 2014;67(5):53-54.
2. Truong VV, Tanemura S, Haché A, Miao L. Optical Properties of Thin Films. Optical Properties of Materials and Their Applications: Wiley; 2019. p. 403-434.
3. Efros AL, Brus LE. Nanocrystal Quantum Dots: From Discovery to Modern Development. ACS Nano. 2021;15(4):6192-6210.
4. Hu H, Zhang W. Synthesis and properties of transition metals and rare-earth metals doped ZnS nanoparticles. Opt Mater. 2006;28(5):536-550.
5. Inamdar AI, Lee S, Kim D, Gurav KV, Kim JH, Im H, et al. Metal-doped ZnS(O) thin films on glass substrates using chemical bath deposition. Thin Solid Films. 2013;537:36-41.
6. Cheng J, Fan D, Wang H, Liu B, Zhang Y, Yan H. Chemical bath deposition of crystalline ZnS thin films. Semicond Sci Technol. 2003;18(7):676-679.
7. Ben Nasr T, Kamoun N, Kanzari M, Bennaceur R. Effect of pH on the properties of ZnS thin films grown by chemical bath deposition. Thin Solid Films. 2006;500(1-2):4-8.
8. Xu X, Bullock J, Schelhas LT, Stutz EZ, Fonseca JJ, Hettick M, et al. Chemical Bath Deposition of p-Type Transparent, Highly Conducting (Cu_x)(ZnS)_{1-x} Nanocomposite Thin Films and Fabrication of Si Heterojunction Solar Cells. Nano Lett. 2016;16(3):1925-1932.
9. Yang H, Holloway PH. Electroluminescence from Hybrid Conjugated Polymer–CdS:Mn/ZnS Core/Shell Nanocrystals Devices. The Journal of Physical Chemistry B. 2003;107(36):9705-9710.
10. Hubert C, Naghavi N, Canava B, Etcheberry A, Lincot D. Thermodynamic and experimental study of chemical bath deposition of Zn(S,O,OH) buffer layers in basic aqueous ammonia solutions. Cell results with electrodeposited CuIn(S,Se)₂ absorbers. Thin Solid Films. 2007;515(15):6032-6035.
11. Jrad A, Ben Nasr T, Turki-Kamoun N. Study of structural, optical and photoluminescence properties of indium-doped zinc sulfide thin films for optoelectronic applications. Opt Mater. 2015;50:128-133.
12. Ni W-S, Lin Y-J. Defect-induced magnetic properties of Cu-doped ZnS films with different copper contents. J Alloys Compd. 2015;649:968-972.
13. Kouklin N. Cu-Doped ZnO Nanowires for Efficient and Multispectral Photodetection Applications. Adv Mater. 2008;20(11):2190-2194.
14. Motaung DE, Kortidis I, Mhlongo GH, Duvenhage M-M, Swart HC, Kiriakidis G, et al. Correlating the magnetism and gas sensing properties of Mn-doped ZnO films enhanced by UV irradiation. RSC Advances. 2016;6(31):26227-26238.
15. Goktas A, Aslan F, Tumbul A. Nanostructured Cu-doped ZnS polycrystalline thin films produced by a wet chemical route: the influences of Cu doping and film thickness on the structural, optical and electrical properties. J Sol-Gel Sci Technol. 2015;75(1):45-53.
16. Chalana SR, Jolly Bose R, Reshmi Krishnan R, Kavitha VS, Sreeja Sreedharan R, Mahadevan Pillai VP. Structural phase modification in Cu incorporated nanostructured zinc sulfide thin films. Journal of Physics and Chemistry of Solids. 2016;95:24-36.
17. Alqahtani MS, Hadia NMA, Mohamed SH. Controlled synthesis, morphological, optical and electrical properties of copper-doped zinc oxysulfide nanostructures. Appl Phys A. 2018;124(9).
18. Sreedhar M, Neelakanta Reddy I, Bera P, Shyju TS, Anandan C. Studies of Cu-doped ZnS thin films prepared by sputtering technique. Surf Interface Anal. 2016;49(4):284-290.
19. Kryshab T, Khomchenko VS, Andraca-Adame JA, Zavyalova LV, Roshchina NN, Rodionov VE, et al. Preparation and properties of thin ZnS:Cu films phosphors. Thin Solid Films. 2006;515(2):513-516.
20. Nikzad M, Khanlary MR, Rafiee S. Structural, optical and morphological properties of Cu-doped ZnS thin films synthesized by sol–gel method. Appl Phys A. 2019;125(8).
21. V S GK, Maidur SR, Patil PS, M.G M. Role of copper dopant in two-photon absorption and nonlinear optical properties of sprayed ZnS thin films for optical limiting applications. Phys Lett A. 2021;398:127276.
22. Sahraei R, Noshadi S, Goudarzi A. Growth of nanocrystalline CuS thin films at room temperature by a facile chemical deposition method. RSC Advances. 2015;5(94):77354-77361.
23. Piryaei M, Gholami Hatam E, Ghobadi N. Influence of pH on the optical, structural and compositional properties of nanocrystalline CdSe thin films prepared by chemical bath deposition. Journal of Materials Science: Materials in Electronics. 2016;28(3):2550-2556.
24. Jrad A, Naffouti W, Ben Nasr T, Ammar S, Turki-Kamoun N. Effect of manganese concentration on physical properties of ZnS:Mn thin films prepared by chemical bath deposition.

- Journal of Materials Science: Materials in Electronics. 2016;28(2):1463-1471.
25. Ulutas C, Guneri E, Kirmizigul F, Altindemir G, Gode F, Gumus C. γ -MnS thin films prepared by chemical bath deposition: Effect of bath temperature on their physical properties. *Materials Chemistry and Physics*. 2013;138(2-3):817-822.
 26. Jayanthi K, Chawla S, Chander H, Haranath D. Structural, optical and photoluminescence properties of ZnS:Cu nanoparticle thin films as a function of dopant concentration and quantum confinement effect. *Cryst Res Technol*. 2007;42(10):976-982.
 27. Muthukumar S, Ashok kumar M. Structural, FTIR and photoluminescence properties of ZnS:Cu thin films by chemical bath deposition method. *Mater Lett*. 2013;93:223-225.
 28. Ortiz-Ramos DE, González LA, Ramirez-Bon R. p-Type transparent Cu doped ZnS thin films by the chemical bath deposition method. *Mater Lett*. 2014;124:267-270.
 29. Jrad A, Naffouti W, Nefzi C, Ben Nasr T, Ammar S, Turki-Kamoun N. Effect of copper concentration on the physical properties of ZnS:Cu alloys prepared by chemical bath deposition. *Journal of Materials Science: Materials in Electronics*. 2016;27(10):10684-10695.
 30. Virpal, Hastir A, Sharma S, Singh RC. Structural, optical and dielectric properties of lead doped ZnS nanoparticles. *Appl Surf Sci*. 2016;372:57-62.
 31. Soheyli E, Sahraei R, Nabiyouni G. Aqueous based synthesis of N-acetyl- L -cysteine capped ZnSe nanocrystals with intense blue emission. *Opt Mater*. 2016;60:564-570.
 32. Nilsen WG. Raman Spectrum of Cubic ZnS. *Phys Rev*. 1969;182(3):838-850.
 33. Chamorro W, Shyju TS, Boulet P, Migot S, Ghanbaja J, Miska P, et al. Role of Cu⁺ on ZnS:Cu p-type semiconductor films grown by sputtering: influence of substitutional Cu in the structural, optical and electronic properties. *RSC Advances*. 2016;6(49):43480-43488.
 34. Jin P-J, Yao Z-Q, Zhang M-L, Li Y-H, Xing H-P. A pigment (CuS) identified by micro-Raman spectroscopy on a Chinese funerary lacquer ware of West Han Dynasty. *J Raman Spectrosc*. 2009;41(2):222-225.
 35. Hodes G. *Chemical Solution Deposition Of Semiconductor Films*: CRC Press; 2002 2002/10/08.
 36. Goudarzi A, Aval GM, Park SS, Choi M-C, Sahraei R, Ullah MH, et al. Low-Temperature Growth of Nanocrystalline Mn-Doped ZnS Thin Films Prepared by Chemical Bath Deposition and Optical Properties. *Chem Mater*. 2009;21(12):2375-2385.
 37. Sahraei R, Darafarin S. An investigation on optical characteristics of nanocrystalline ZnS:Ni thin films prepared by chemical deposition method. *Spectrochimica Acta Part A: Molecular and Biomolecular Spectroscopy*. 2015;149:941-948.
 38. Pejova B, Grozdanov I. Structural and optical properties of chemically deposited thin films of quantum-sized bismuth(III) sulfide. *Materials Chemistry and Physics*. 2006;99(1):39-49.
 39. Pankove JI, Kiewit DA. *Optical Processes in Semiconductors*. *J Electrochem Soc*. 1972;119(5):156C.
 40. Soheyli E, Hekmatshoar MH, Parcham F. Optical and structural characterization of quadruplet and quintuplet molybdenum-containing phosphate glasses. *Mod Phys Lett B*. 2016;30(18):1650270.
 41. Darafarin S, Sahraei R, Daneshfar A. Effect of deposition temperature on structural and optical properties of chemically grown nanocrystalline Ni doped ZnS thin films. *J Alloys Compd*. 2016;658:780-787.
 42. Sreeja R, Sridharan K, Philip R, Jayaraj MK. Impurity mediated large three photon absorption in ZnS:Cu nanophosphors. *Opt Mater*. 2014;36(5):861-866.
 43. Kumar SS, Khadar MA, Dhara SK, Ravindran TR, Nair KGM. Photoluminescence and Raman studies of ZnS nanoparticles implanted with Cu⁺ ions. *Nuclear Instruments and Methods in Physics Research Section B: Beam Interactions with Materials and Atoms*. 2006;251(2):435-440.
 44. Kole AK, Kumbhakar P, Chatterjee U. Observation of nonlinear absorption and visible photoluminescence emission in chemically synthesized Cu²⁺ doped ZnS nanoparticles. *Appl Phys Lett*. 2012;100(1):013103.
 45. Peng WQ, Cong GW, Qu SC, Wang ZG. Synthesis of shuttle-like ZnO nanostructures from precursor ZnS nanoparticles. *Nanotechnology*. 2005;16(9):1469-1473.
 46. Denzler D, Olschewski M, Sattler K. Luminescence studies of localized gap states in colloidal ZnS nanocrystals. *J Appl Phys*. 1998;84(5):2841-2845.
 47. Haddad H, Chelouche A, Talantikite D, Merzouk H, Boudjouan F, Djouadi D. Effects of deposition time in chemically deposited ZnS films in acidic solution. *Thin Solid Films*. 2015;589:451-456.
 48. Norris DJ, Efron AL, Erwin SC. Doped Nanocrystals. *Science*. 2008;319(5871):1776-1779.